RSC Advances

PAPER

View Article Online
View Journal | View Issue

Cite this: *RSC Adv.*, 2022, **12**, 18412

In vitro and *in silico* studies of SARS-CoV-2 main protease M^{pro} inhibitors isolated from *Helichrysum bracteatum*†

Gehad Abdel Wahab, Walaa S. Aboelmaaty, Mohamed Farid Lahloub and Amal Sallam *

Discovering SARS-CoV-2 inhibitors from natural sources is still a target that has captured the interest of many researchers. In this study, the compounds (**1–18**) present in the methanolic extract of *Helichrysum bracteatum* were isolated, identified, and their *in vitro* inhibitory activities against SARS-CoV-2 main protease (M^{pro}) was evaluated using fluorescence resonance energy transfer assay (FRET-based assay). Based on 1D and 2D spectroscopic techniques, compounds (**1–18**) were identified as 24-β-ethyl-cholesta-5(6),22(23),25(26)-triene-3-ol (**1**), α-amyrin (**2**), linoleic acid (**3**), 24-β-ethyl-cholesta-5(6),22(23),25(26)-triene-3-*O*-β-D-glucoside (**4**), 1,3-propanediol-2-amino-1-(3′,4′-methylenedioxyphenyl) (**5**), (−)-(7*R*,8*R*,8′*R*)-acuminatolide (**6**), (+)-piperitol (**7**), 5,7,4′-trihydroxy-8,3′-dimethoxy flavanone (**8**), 5,7,4′-trihydroxy-6-methoxy flavanone (**9**), 4′,5-dihydroxy-3′,7,8-trimethoxyflavone (**10**), 5,7-dihydroxy-3′,4′,5′,8-tetramethoxy flavone (**11**), 1,3-propanediol-2-amino-1-(4′-hydroxy-3′-methoxyphenyl) (**12**), 3′,5′,5,7-tetrahydroxy-6-methoxyflavanone (**13**), simplexoside (piperitol-*O*-β-D-glucoside) (**14**), pinoresinol monomethyl ether-β-D-glucoside (**15**), orientin (**16**), luteolin-3′-*O*-β-D-glucoside (**17**), and 3,5-dicaffeoylquinic acid (**18**). Compounds **6**, **12**, and **14** showed comparable inhibitory activities against SARS-CoV-2 M^{pro} with IC_{50} values of 0.917 ± 0.05, 0.476 ± 0.02, and 0.610 ± 0.03 μM, respectively, compared with the control lopinavir with an IC_{50} value of 0.225 ± 0.01 μM. The other tested compounds showed considerable inhibitory activities. The molecular docking study for the tested compounds was carried out to correlate their binding modes and affinities for the SARS-CoV-2 M^{pro} enzyme with the *in vitro* results. Analyzing the results of the *in vitro* assay together with the obtained *in silico* results led to the conclusion that phenylpropanoids, lignans, and flavonoids could be considered suitable drug leads for developing anti-COVID-19 therapeutics. Moreover, the phenylpropanoid skeleton oxygenated at C3, C4 of the phenyl moiety and at C1, C3 of the propane parts constitute an essential core of the SARS-CoV-2 M^{pro} inhibitors, and thus could be proposed as a scaffold for the design of new anti-COVID-19 drugs.

Received 23rd February 2022
Accepted 8th June 2022

DOI: 10.1039/d2ra01213h

rsc.li/rsc-advances

1. Introduction

Severe acute respiratory syndrome coronavirus 2 (SARS-CoV-2) is a novel strain of the coronavirus group. It emerged in the city of Wuhan, China at the end of 2019, causing an outbreak of unusual viral pneumonia. It caused acute respiratory disease that was named coronavirus disease 2019 (COVID-19) by the WHO on 11 February 2020. Being highly transmissible and pathogenic such that it has spread fast all over the world, WHO defined it on 11 March 2020 as a pandemic, posing an extraordinary threat to global public health.[1] To date, there are no generally proven antiviral drugs against SARS-CoV-2, although several clinical trials all over the world are testing several known antiviral drugs.[2] Therefore, finding natural, semisynthetic, or synthetic remedies for COVID-19 is the target of many researches now.

The main protease (M^{pro}), papain-like protease (PL^{pro}), and RNA-dependent RNA polymerase (RdRp) of SARS-CoV-2 are considered decisive factors in the infectious route of the virus; they have been reported as important targets for therapeutic strategies.

SARS-CoV-2 main protease (M^{pro}) or (3-chymotrypsin-like protease $3CL^{pro}$) is an enzyme responsible for the proteolysis and release of essential functioning peptides, playing a great role in replication, and thus the life cycle of the virus.[2–5] Moreover, M^{pro} is highly conserved across coronaviruses; thus, inhibiting main proteases is considered an attractive target for the discovery of effective antiviral drugs for the treatment of not only SARS-CoV-2 but also other coronaviruses.[6] Although

Pharmacognosy Department, Faculty of Pharmacy, Mansoura University, Mansoura, 35516, Egypt. E-mail: asallam@mans.edu.eg; gehadabdelwahab@mans.edu.eg; algehadalhaq@yahoo.com; walaa_safwat@mhans.edu.eg; walaa_m_s@yahoo.com; mfilah@yahoo.com; Fax: +20502247496; Tel: +201092017949

† Electronic supplementary information (ESI) available. See https://doi.org/10.1039/d2ra01213h

researchers have focused their efforts on studying the potential antiviral properties of plants and their constituents from different classes including flavonoids and lignans as anti-COVID-19 agents through *in silico* studies targeting M^{pro} and other enzymes, little has been found concerning the *in vitro* studies.[4–7]

The genus *Helichrysum* belonging to family *Asteraceae* (*Compositae*) includes approximately 600 species spread widely all over the world, especially in the Southern Hemisphere; it is also widespread through Eurasia, Australia, and the Mediterranean region.[8–13] Several classes of phytoconstituents have been reported in different *Helichrysum* species, mainly phenolics, lignans, phloroglucinols, pyrones, fatty acids, and terpenoid compounds.[11,12] Since ancient times, *Helichrysum* species are well known for their medicinal properties as diuretic, anti-inflammatory, hepatoprotective, and anti-psoriasis. Also, they have been used in treatment of colds, cough, inflammation, and allergy conditions such as those related to the respiratory tract.[11,12]

It is reported that several species of genus *Helichrysum* show antiviral activities against different viruses including coronaviruses or similar viruses. *H. arenarium* showed antiviral activities against Herpes simplex virus Type-1 (HSV-1) and Para-influenza-3. *H. italicum* and *H. auronitens* have antiviral activities against HSV-1, while *H. melanacme* has antiviral activity against HIV.[9,10,13–15] Helichrysetin, a chalcone derivative found within numerous *Helichrysum* species, was reported to be able to inhibit MERS-CoV $3CL^{pro}$.[15]

H. bracteatum is known as straw flower and is widely cultivated as an ornamental plant.[16,17] Previous phytochemical studies have reported the presence of different classes of compounds as flavonoids, lignans, and phenolic acids.[17–19]

This study is concerned with discovering potential antiviral leads against COVID-19 based on the evaluation of the ability of *H. bracteatum* methanolic extract, as well as fractions and isolated phytoconstituents to inhibit SARS-CoV-2 main protease (M^{pro}) through *in vitro* and *in silico* studies.

2. Results and discussion

2.1 Characterization of the isolated compounds

Phytochemical investigation of petroleum ether, methylene chloride, and ethyl acetate fractions of the methanolic extract of *H. bracteatum* leaves resulted in the isolation and structure elucidation of eighteen compounds (**1–18**) (Fig. 1) including two steroidal compounds (**1**,**4**), one pentacyclic triterpene (**2**), one fatty acid (**3**), two phenyl propanoid derivatives nitrogenated at C2 (**5**,**12**), four lignans (**6**,**7**,**14**,**15**), seven flavonoids, three flavanones (**8**,**9**,**13**), four flavones (**10**,**11**,**16**,**17**), and one phenolic acid derivative (**18**). The proton and carbon values beside the spectra of the isolated compounds are present in the ESI file (Data S1 and Fig. S1–S50†).

Compounds (**1–4**) were isolated from the petroleum ether fraction. They were confirmed from their proton and carbon chemical shift values (Fig. S1–S8†) compared with those reported in the literature. They were identified as 24-β-ethyl-cholesta-5(6),22(23),25(26)-triene-3-ol (**1**) and its glucoside 24-β-ethyl-cholesta-5(6),22(23),25(26)-triene-3-*O*-β-D-glucoside (**4**),[20] besides α-amyrin (**2**),[21,22] and linoleic acid (**3**).[23] It is the first time that compounds **1** and **4** have been isolated from family *Compositae*. It is the first time that compound **2** has been isolated from genus *Helichrysum*. Compound **3** was previously reported from *Helichrysum* seed oil.[24]

Compounds **5** and **12** were concluded to be phenyl propanoid derivatives nitrogenated at C2. The careful examination of the ^{1}H-NMR spectrum of compound **5** (Fig. S9†) showed signals at δ_H 6.78 (br d, 1H, $J = 8$, H-5′), δ_H 6.80 (br d, 1H, $J = 10.8$, H-6′), and δ_H 6.85 (br s, 1H, H-2′), indicating the possible presence of the tri-substituted phenyl ring. It also showed the signal of an oxygenated methylene that may represent a methylenedioxy group at δ_H 5.95 (s, 2H), substituting the phenyl ring. Signals representing one oxygenated methine proton at δ_H 4.72 (d, 1H, $J = 3.2$, H-1) and one aminomethine proton δ_H 3.05 (m, 1H, H-2) besides an oxygenated methylene group at δ_H 4.23 (dd, 1H, $J_1 = 6.4$ & 8.4, H-3a) and δ_H 3.87 (dd, 1H, $J = 6.8$ & 2, H-3b) were also observed, indicating the possible presence of the 1,3-dihydroxy-2-amino-propane moiety. The APT spectrum (Fig. S10†) showed signals supporting the previous possibilities. It revealed two oxygenated quaternary aromatic carbon signals at δ_C 148.0 (C-3′) & 147.1 (C-4′), a quaternary aromatic carbon at δ_C 135.0 (C-1′), and three aromatic methine carbons at δ_C 106.5 (C-2′), 108.2 (C-5′), and 119.4 (C-6′). It also showed carbon signals representing oxygenated methylene carbon at δ_C 101.1, indicating the presence of the methylenedioxy group substituting the phenyl ring. Moreover, it showed signals representing one oxygenated aliphatic methine carbon at δ_C 85.8 (C-1) and one oxygenated methylene carbon at δ_C 71.7 (C-3) and one aminomethine carbon at δ_C 54.3 (C-2), which was shifted upfield than the oxygenated carbons (C-1 & 3), thus confirming the presence of the 1,3-dihydroxy-2-amino-propane moiety. The HMBC spectrum (Fig. S11†) showed a cross peak correlating the proton signal at δ_H 4.71 (H-1) with the quaternary carbon signals at δ_C 135.0 (C-1′), 106.5 (C-2′), and 119.4 (C-6′). This indicated that the 1,3-dihydroxy-2-amino-propane moiety substituted the phenyl ring at C-1′. The HMBC cross peaks from the methylenedioxy group δ_H 5.95 to carbons δ_C 148.0 (C-3′) & 147.1 (C-4′) confirmed that the methylendioxy group is substituting the phenyl ring at C-3′ & 4′. Compound **5** was identified as 1,3-propanediol-2-amino-1-(3′,4′-methylenedioxyphenyl). It was previously isolated only from *Artemisia selengensis* F. *Compositae*;[25] also, it was reported as a synthetic compound.[26]

The careful examination of the ^{1}H-NMR and APT spectra of compound **12** (Fig. S26 and S27†) indicated that it is also a phenyl propanoid derivative nitrogenated at C2. Comparing its ^{1}H-NMR and APT spectra with those of compound **5** revealed that compound **12** was similar to compound **5**, but the phenyl ring is substituted with methoxy and hydroxy groups instead of methylenedioxygroup (at C-3′, 4′). Compound **12** was identified as 1,3-propanediol-2-amino-1-(4′-hydroxy-3′-methoxyphenyl).[27] It was previously isolated only from *Santolina chamaecyparissus* F. *Compositae* and our study reports its detailed chemical shift values for the first time.

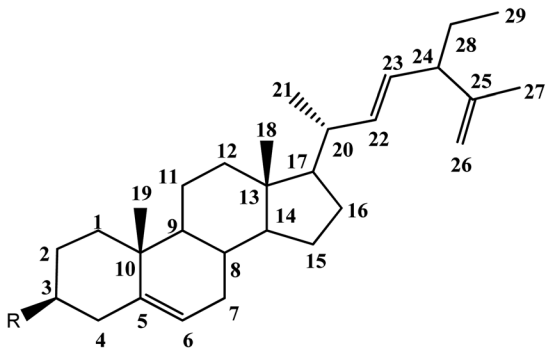

R= OH……..... 1
R= O-*B*-D-glucose…… 4

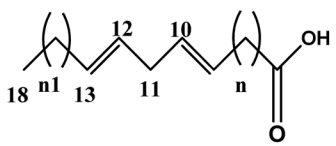

n=7& n1= 4..... 3

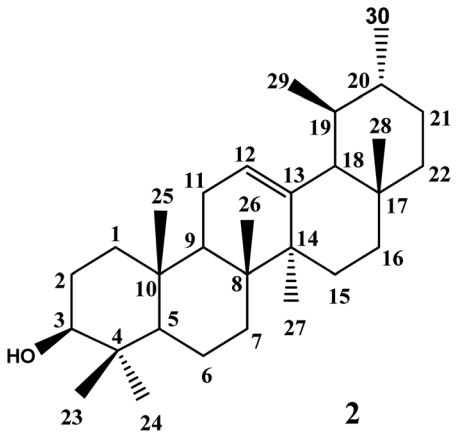

2

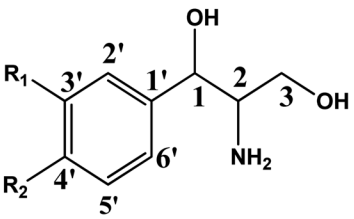

R_1, R_2= —OCH_2O—…. 5
R_1= OCH_3, R_2= OH….12

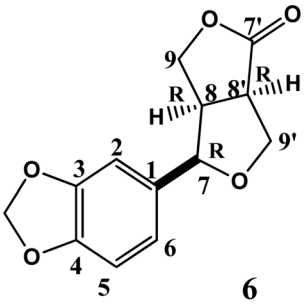

6

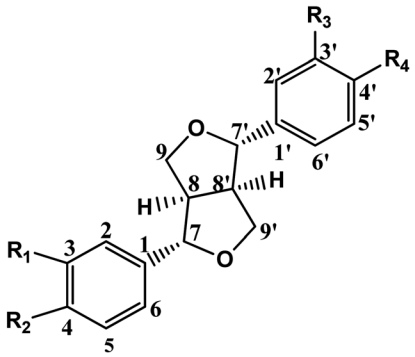

R_1, R_2=—OCH_2O- , R_3= OCH_3, R_4= OH…….. 7
R_1, R_2=—OCH_2O- , R_3= OCH_3, R_4= O-*B*-D-glucoside ……. 14
R_1, R_2, R_3= OCH_3, R_4= O-*B*-D-glucose……. 15

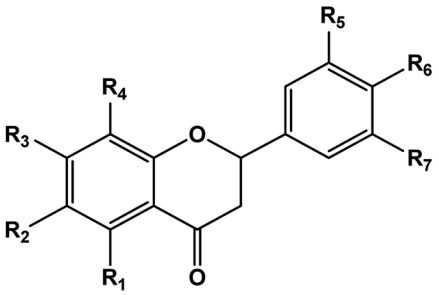

R_1= R_3= R_6= OH, R_4= R_5= OCH_3, R_2= R_7= H …… 8
R_1= R_3= R_6= OH, R_2= OCH_3, R_4= R_5= R_7= H …….9
R_1= R_3= R_5= R_7= OH, R_2= OCH_3, R_4= R_6= H ….. 13

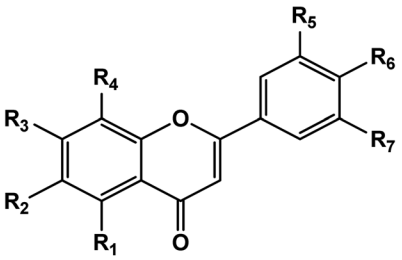

R_1= R_6= OH, R_3= R_4= R_5= OCH_3, R_2= R_7= H ……..... 10
R_1= R_3= OH, R_4= R_5= R_6= R_7= OCH_3, R_2= H ……..... 11
R_1= R_3= R_5= R_6= OH, R_4= C-*B*-D-glucose, R_2= R_7= H …… 16
R_1= R_3= R_6= OH, R_2= R_4=R_7= H, R_9= O-*B*-D-glucose ……..17

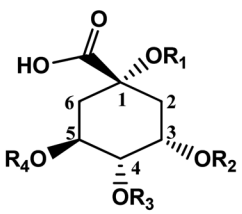

R_1= R_3= H, R_2= R_4=caffeoyl
18

Fig. 1 Structures of compounds (1–18).

Compounds **7**, **14**, and **15** were found to be furofuranlignans. Comparing the data obtained from ^{1}H-NMR and APT spectra (Fig. S14 and S15†) with that reported in the previous literature and the stereochemistry reported for furofuranlignans,[28–30] compound **7** was identified as (+)-piperitol.[31,32] Compound **14** was found to be the glucoside of **7**; this was revealed by its ^{1}H-

NMR and APT spectra (Fig. S40 and S41†), which showed the doublet signal representing the anomeric proton (H-1″) at 4.88 ppm (1H, d, $J = 6.7$ Hz) in addition to the carbon signal at δ_C 100.6 (C-1″) and the four hydroxylated aliphatic methine carbons at δ_C 71.6, 77.3, 70.1, 77.4, besides the hydroxylated aliphatic methylene carbon at δ_C 61.1 (C-6″), indicating the presence of the hexose sugar glucose. Compound **14** was identified as simplexoside (piperitol-*O*-β-D-glucoside).[33,34] Both compounds **7** & **14** were previously isolated from *H. bracteatum* aerial parts.[17] A careful examination of the ^{1}H-NMR and APT spectra of compounds **14** & **15** (Fig. S40–S43†) revealed that compound **15** is similar to compound **14**, except for the presence of two signals at δ_H 3.76 (6H, s, OCH_3-3 & OCH_3-4), representing two methoxy groups instead of the signal at 6.00 (2H, s, OCH_2O), thus representing the methylenedioxy group in compound **14**. Compound **15** was identified as pinoresinol monomethyl ether-β-D-glucoside.[35] Compound **15** is isolated from F. *Compositae* (*Asteraceae*) for the first time in this study. Comparing the ^{1}H-NMR and APT spectra of compound **6** (Fig. S12 and S13†) with compound **7** revealed that **6** is similar to **7**, but it lacks the presence of one aryl group; instead, it showed a carbonyl moiety. This was deduced from the carbonyl group at δ_C 178.1 corresponding to C-7′. Comparing this data with the previous literature, compound **6** was identified as (−)-(7*R*,8*R*,8′*R*)-acuminatolide.[36] To the best of our knowledge, acuminatolide was previously isolated from aerial parts of *H. acuminatum*.[37]

Compounds **8**, **9**, and **13** were found to be flavanones depending on the common characteristic features that appeared in the UV-spectral data besides both ^{1}H-NMR and APT data. The UV-spectra of these three compounds showed two absorption bands, band I in the λ_{max} range of 289–291 nm and band II in the λ_{max} range of 232–236 nm, which appeared to be in agreement with those characteristic for flavanones or dihydroflavonols.[38,39] The ^{1}H-NMR spectra of the three compounds (Fig. S16, S19 and S28†) revealed the presence of two double doublet signals characteristic for H-3α and H-3β in the range of δ_H 2.5–3.01 besides one double of doublet signal corresponding to the oxygenated methine H-2 at δ_H 5.20. The APT spectra of the three compounds (Fig. S17, S20 and S31†) supported this deduction by showing signals representing carbonyl (C-4) in the range of δ_C 195.2–197.2, a signal for the methylene group at 42.7 (C-3), besides the signal representing oxygenated methine (C-2) at δ_c 79.2.[40]

The UV spectral data in different shift reagents (Table S1†) suggested that **8** has a flavanone structure with free OH groups at positions 5, 7, and 4′.[38] The ^{1}H-NMR spectrum (Fig. S16†) showed a signal at δ_H 5.18 (1H, dd, $J = 2.8$ & 12.6) representing the oxygenated methine H-2 and pair of double doublets at δ_H 2.56 (1H, dd, $J = 2.8$ & 17.2) and δ_H 2.97 (1H, dd, $J = 12.8$ & 17.2) representing the methylene protons H-3α and 3β, respectively. These signals are characteristic of the flavanone skeleton. Also, it revealed a singlet signal at δ_H 5.79 (1H, s, H-6), indicating that ring A has only one free proton. Besides, the signals representing the ABX system in ring B that were obtained at δ_H 6.97 (1H, d, $J = 1.6$, H-2′), δ_H 6.71 (1H, d, $J = 8$, H-5′), and δ_H 6.81 (1H, dd, $J = 8.2$ & 2, H-6′). In addition, it showed two signals of two methoxy groups at δ_H 3.66 & 3.78. The APT spectrum (Fig. S17†) showed six oxygenated aromatic carbon signals along with a carbonyl signal in the range of δ_C 130–200 ppm. The presence of a carbonyl signal at δ_C 195.7 (C-4), an oxygenated methine signal at δ_C 79.2 (C-2) and a methylene signal at 42.7 (C-3) confirmed the flavanone skeleton.[40,41] There were three signals representing the oxygenated aromatic carbons substituted with free hydroxyl groups at δ_C 159.0, 164.6, & 146.6 representing C-5, 7, & 4′, respectively, which were confirmed previously by UV data; the other two signals were methoxylated, one at δ_C 147.7 representing C-3′ as ring B showed an ABX system with free OH at C-4′ only. The other one at δ_C 130.7 represents C-8 rather than C-6 that was not substituted and appeared at δ_C 96.3. Reviewing previous literature that reported flavanone oxygenated at C-8 while C-6 is free and those reported compounds oxygenated at C-6 while C-8 is free, it could be noticed that when C-8 is oxygenated while C-6 is free, C-6 appears at a chemical shift value that is slightly downfield shifted (δ_C 96.3 as in compound **8**) compared with the chemical shift of C-8 if it is free and C-6 is oxygenated, where C-8 in this case appears slightly shifted upfield[41,42] (Table S2†). The data obtained from UV, ^{1}H-NMR, and APT suggested that compound **8** is a flavanone hydroxylated at 5, 7, & 4′ and methoxylated at 8 and 3′. The HMBC spectrum of compound **8** (Fig. S18†) showed cross peaks correlating the methoxy group proton signal at δ_H 3.66 ($H\text{-}R_4$) with the carbon signal at δ_C 130.7 (C-8); also, it showed cross peaks correlating the methoxy group proton signal at δ_H 3.78 ($H\text{-}R_5$) with the carbon signal at δ_C 147.7 (C-3′). These data confirmed that both C-8 and 3′ are blocked with OCH_3 groups, while C-5, 7, and 4′ are substituted with free hydroxyl groups. Also, it showed cross peaks correlating the methine H-6 at δ_H 5.79 with the carbon signals at δ_C 159.0 (C-5), 130.7 (C-8), & 100.7 (C-10), which also supports this hypothesis. The previous data suggests that compound **8** is 5,7,4′-trihydroxy-8,3′-dimethoxy flavanone. Comparing the carbons values obtained from the APT spectrum of compound **8** with previous literature revealed that compound **8** is 5,7,4′-trihydroxy-8,3′-dimethoxy flavanone.[41] It worth noting that this is the first study that reports the isolation of compound **8** (5,7,4′-trihydroxy-8,3′-dimethoxy flavanone) from the family *Compositae*. It was previously isolated from *Iris unguicularis*[43] and our study reports its detailed chemical shift values.

Comparing the proton and carbon values of compound **9** obtained from ^{1}H-NMR and APT spectra (Fig. S19 and S20†) with those of compound **8** revealed that compound **9** is similar to compound **8** with the presence of the methoxy group at C-6 rather than C-8 (owing to the slightly upfield shifted value of C-8 at δ_c 94.8 compared to the value of the unsubstituted C-6, which is slightly shifted downfield when unsubstituted at δ_C 96.3 as in compound **8**) and the absence of the methoxy group at C-3′ (Fig. S19, S20 and Table S2†). Thus, compound **9** was identified as 5,7,4′-trihydroxy-6-methoxy flavanone and it is the first time to be isolated from F. *Compositae* in this study.[41,42]

The molecular formula of compound **13** was determined to be $C_{16}H_{14}O_7$ from the $[M + H]^+$ peak at *m*/*z* 319.24 appearing in the LC-ESI$^+$-MS spectrum (Fig. S36†), which is in agreement with the calculated one at *m*/*z* 319.28. The UV spectral data in

different shift reagents (Table S1†) indicated that **13** has a flavanone structure with free OH groups at positions 5 and 7.[38] Comparing the proton and carbon chemical shift values of ring A in compound **13** obtained from ^{1}H-NMR and APT spectra (Fig. S28–S31, S38 and Table S2†) with those of compound **9** revealed that both compounds show the same substitution patterns in ring A (5,7-dihydroxy & 6-methoxy). The ^{1}H-NMR, APT, & HSQC spectra showed signals characteristic for the flavanone skeleton at δ_H 5.16 (1H, dd, J = 2.8 & 12.8) representing the oxygenated methine H-2 correlated to δ_c 79.2, a pair of double doublets at δ_H 2.60 (1H, dd, J = 2.8 & 17.2), and δ_H 2.96 (1H, dd, J = 12.8 & 17.2) representing methylene protons H-3α and 3β, respectively, which are correlated to δ_C 42.7 besides the carbonyl at δ_C 197.2 (C-4).[40,41] The singlet signal at δ_H 5.87 (1H, s, H-8) correlated to δ_c 94.8 and a methoxy group at $\delta_{H/C}$ 3.68/59.6 were also present. Singlet signals representing three protons of ring B at δ_H 6.68 (2H, s) and δ_H 6.81 (1H, s) representing H-2′, 4′, & 6′ correlated to δ_C 117.9, 114.8, & 113.3, respectively, revealed the absence of AB or ABX system in ring B. This suggestion was supported by the HMBC cross peaks from δ_H 6.68 (H-2′) & 6.81 (H-6′) to the carbon signal at δ_C 79.2 (C-2) and from δ_H 6.68 & 6.81 (H-2′& H-6′) to δ_C 114.8(C-4′) (Fig. S34 and S35†). The APT spectrum (Fig. S31†) showed also six oxygenated aromatic carbon signals along with a carbonyl one in the range of δ_C 129–200 ppm. The carbon signal at δ_C 129.0 is methoxylated rather than hydroxylated; this could be detected from the HMBC spectrum (Fig. S34†) that showed cross peaks correlating the methoxyprotons at δ_H 3.68 with the carbon signal at δ_c 129.0. The carbon signal representing the methoxylated aromatic carbon at δ_C 129.0 was assigned to C-6 rather than C-8 that was not substituted and appeared at a slightly upfield chemical shift value (δ_H 94.3, as C-8 of compound **9**) when compared with the chemical shift value of the unsubstituted C-6 that appeared at a slightly downfield shifted value (δ_H 96.3, as C-6 in compound **8**)[41,42] (Table S2†). The HMBC spectrum showed cross peaks correlating the signal at δ_H 5.87 (H-8) with carbon signals at δ_C 129.0 (C-6), 158.8 (C-9), 159.5 (C-7), & 102.1 (C-10). The hydroxylated carbon signals at δ_C 155.2 & 159.5 were assigned to C-5 & 7. The remaining oxygenated carbon signals at δ_C 145.1 & 145.5 were assigned to the hydroxylated carbons in ring B. Lacking an AB or ABX system in ring B and absence of free hydroxyl group at C-4′ (according to UV data) suggested rare substitution by the hydroxyls at C-3′ & C-5′ not the common one at C-3′ & C-4′ in ring B. This suggestion was supported by the HMBC correlation from δ_H 6.68 (H-2′) to δ_C 145.1 (C-3′) and from δ_H 6.81 (H-6′) to δ_C 145.5 (C-5′) (Fig. S34†). The ESI$^+$-MS fragmentation of compound **13** showed a base peak at m/z 183.61 $[M + H]^+$ corresponding to the fragment (a) 3-(3,5-dihydroxyphenyl)propanoic acid fragment (calculated m/z 183.18), confirming that ring B is disubstituted by two hydroxyl groups (Fig. S37A and B†). The previous data suggested that compound **13** is 5,7,3′,5′-tetrahydroxy-6-methoxy flavanone. Reviewing the current literature, it was found that this study is the first to report the isolation of 5,7,3′,5′-tetrahydroxy-6-methoxy flavanone from F. *Compositae* (*Asteraceae*). It was previously isolated only from *Salvia plebeian* F. *Labiatae*;[44] also, it was reported as a semi-synthetic compound.[45] This study is the first that reports detailed data for that rare substituted flavanone at C-3′ & 5′.

The careful examination of the UV, ^{1}H-NMR, and APT spectra of compounds **10** & **11** indicated that they are flavones. They were identified as 4′,5-dihydroxy-3′,7,8-trimethoxyflavone (**10**) and 5,7-dihydroxy-3′,4′,5′,8-tetramethoxy flavone (**11**). This was deduced from the UV-spectra of the two compounds that showed two absorption bands, band I in the λ_{max} range of 323–345 nm and band II in the λ_{max} range of 276–278 nm, which appear to be in agreement with those characteristic for flavones.[38,39] The ^{1}H NMR spectra of the two compounds (Fig. S21 and S24†) revealed the presence of a singlet signal corresponding to the methine proton H-3 at (δ_H 6.99 & 6.62 for compounds **10** & **11**, respectively). The APT spectra of the two compounds (Fig. S22 and S25†) supported this deduction by showing signals representing carbonyl (C-4) (at δ_C 182.7 & 182.4 for compounds **10** & **11**, respectively) and the signal for the methine carbon C-3 (at δ_C 103.5 & 105.4 for compounds **10** & **11**, respectively).

The UV spectral data in different shift reagents suggested that **10** has a flavone structure with free OH groups at positions 5 and 4′.[38] Both ^{1}H- and DEPT-Q NMR data also supported the previous conclusion. The ^{1}H-NMR spectrum (Fig. S21†) showed two singlet signals at δ_H 6.59 (1H, s, H-6) and 6.99 (1H, s, H-3). Also, it showed signals representing aromatic protons of ring B at δ_H 7.59 (1H, s, H-2′), 7.00 (1H, d, J = 6.7, H-5′), and 7.60 (1H, d, J = 6, H-6′). Besides, it revealed three methoxy groups at δ_H 3.92, 3.86, & 3.90 and carbon signals at δ_C (56.9, 61.6, & 56.5) representing R_3, R_4, & R_5. The DEPT-Q spectrum (Fig. S22†) showed seven oxygenated aromatic carbon signals along with the carbonyl signal in the range of δ_C 125–183 ppm. The presence of a carbonyl signal at δ_C 182.7 (C-4) and a signal at 103.5 (C-3) confirmed the flavone skeleton.[40,41] The two signals at δ_C 164.3 & 151.4 ppm were assigned to the two ether-linked carbons C-2 and C-9, respectively. The two signals of hydroxylated aromatic carbons at δ_C 157.1 & 148.5 were assigned to C-5 & 4′, respectively, which was confirmed from the HMBC spectrum (Fig. S23†) that showed cross peaks correlating δ_H 6.59 (H-6) with both oxygenated carbons at δ_C 128.9 (C-8) & 104.3 (C-10), and the absence of a cross peak with C-9 (δ_C 151.4), confirming that H-8 is blocked. The other three methoxylated aromatic carbon signals at δ_C 158.8, 128.9, & 149.2 were assigned to carbons C-7, 8, & 3′; this was supported by the HMBC cross peaks correlating the methoxy group proton signal at δ_H 3.92 (OCH_3-R_3) with the carbon signal at δ_C 158.8 (C-7). Also, it showed a cross peak correlating the methoxy group proton signal at δ_H 3.86 (OCH_3-R_4) with the carbon signal at δ_C 128.9 (C-8). The third methoxy group at δ_H 3.90 (OCH_3-R_5) showed a cross peak with the carbon signal at δ_C 149.2 (C-3′). The data obtained from UV, ^{1}H, and DEPT-Q spectra revealed that compound **10** is a flavone hydroxylated at position 5 & 4′ and methoxylated at C-7, 8, & 3′. This structure is in agreement with that representing 4′,5-dihydroxy-3′,7,8-trimethoxyflavone. Comparing this data with that reported in the literature, compound **10** could be identified as 4′,5-dihydroxy-3′,7,8-trimethoxyflavone.[41] It is the first report for the isolation of 4′,5-dihydroxy-3′,7, 8-trimethoxyflavone from F. *Compositae*

(*Asteraceae*). It was previously isolated from *Ocimum sanctum* leaves.[46] It was reported as a synthetic compound in a previous study.[47] This study reports its detailed proton and carbon chemical shift values for the first time.

The ^{1}H-NMR spectrum of compound **11** (Fig. S24†) showed one signal at δ_H 7.13 representing the singlet protons (2H-2′, 6′). Besides, it revealed four methoxy groups at δ_H 4.00 (3H, s, R_4), 3.95 (6H, s, R_5 & R_7), & 3.94 (3H, s, R_6). The APT spectrum (Fig. S25†) showed eight oxygenated aromatic carbon signals alongwith the carbonyl signal in the range of δ_C 125–183 ppm. The data obtained from UV, ^{1}H, and APT spectra revealed that compound **11** is a flavone hydroxylated at positions 5 & 7 and methoxylated at 8, 3′, 4′, and 5′. Comparing proton and carbon values of compound **11** with previous literature, compound **11** could be identified as 5,7-dihydroxy-3′,4′,5′,8-tetramethoxy flavone.[41] It is the first time to report the isolation of this compound from family *Compositae*. It was previously isolated from Dikamali gum,[48] which reported it as a semi-synthetic compound;[49] our study is the first to report its detailed chemical shift values.

Careful examination of the UV, ^{1}H-NMR, and APT spectra of compounds **16** & **17** indicated that these compounds are glucosidated flavones. They were identified as orientin (**16**) and luteolin-3′-*O*-β-D-glucoside (**17**). The UV spectra of the two compounds showed two absorption bands, band I in the λ_{max} range of 331–346 nm and band II at λ_{max} 271 nm, which appear to be in agreement with those characteristic for flavones.[38,39] The ^{1}H-NMR spectra of the two compounds (Fig. S44 and S46†) revealed the presence of the singlet signal corresponding to the methine proton H-3 at (δ_H 6.68 & 6.52 for compound **16** & **17**, respectively). The APT spectra of the two compounds (Fig. S45 and S46†) supported this deduction by showing signals representing carbonyl (C-4) at δ_C 182.5 for the two compounds and signal for the methine carbon C-3 (at δ_C 102.9 & 103.7 for compounds **16** & **17**, respectively).

These UV-spectral data in different shift reagents suggested the presence of a flavone structure in **16** with free OH groups at positions 5, 7, 3′, and 4′. The doublet at 4.69 ppm (1H, d, $J = 9.6$ Hz) in addition to the carbon signal at δ_C 73.9 and the four hydroxylated aliphatic methine carbons at δ_C 71.2, 79.2, 71.2, 82.5 besides the hydroxylated aliphatic methylene carbon at δ_C 62.1 indicated the presence of a hexose sugar. The doublet at 4.69 ppm (1H, d, $J = 9.6$) represents the anomeric proton of the glucose sugar (H-1″); this coupling constant ($J = 9.6$) indicates that the sugar is β-linked. The upfield shifted carbon signal at δ_C 73.9 represents the anomeric carbon of the sugar (C-1″) was reported for C-linked-β-D-sugar rather than O-linked-β-D-sugar.[40] The glucose substitutes compound **16** at C-8 rather than C-6 owing to the slight upfield shifted value of the glycosylated C-8 at δ_C 105.0 as in compound orientin compared with the value of the glycosylated C-6, which is slightly downfield shifted at δ_C 108.9 as isoorientin.[38,50] Reviewing the current literature, the data obtained from the UV, ^{1}H, and APT spectra of compound **16** are consistent with those reported for orientin.[50] This study is the first that reports the isolation of orientin from genus *Helichrysum*.

The data obtained from UV spectra in different shift reagents (Table S1†), ^{1}H-NMR, APT, and HMBC spectra (Fig. S46–S48†) of compound **17** are consistent with those reported for luteolin-3′-*O*-β-D-glucoside.[38,40] It was previously isolated from *H. arenarium* flowers.[51]

The careful examination of both ^{1}H-NMR and APT spectra of **18** (Fig. S49 and S50†) showed that compound **18** contains quinic acid nucleus esterified with the two caffeoyl moieties at C-3 & C-5. Thus, compound **18** was identified as 3,5-dicaffeoylquinic acid (isochlorogenic acid).[52] It was previously isolated from *H. bracteatum* flowers and *H. italicum* aerial parts.[18,53]

2.2 Inhibitory activities against SARS-CoV-2 main protease (M^{pro} or $3CL^{pro}$)

Several species of genus *Helichrysum* were reported to have antiviral activities against coronaviruses and other viruses such as Herpes simplex virus Type-1.[10,15] Previous literature reported the ability of helichrysetin, a chalcone derivative isolated from certain *Helichrysum* species, to inhibit MERS-CoV $3CL^{pro}$.[15] Several classes of phytoconstituents as flavonoids and lignans are reported in *in silico* studies as potential anti-COVID-19 agents by inhibiting SARS-CoV-2 main protease (M^{pro}) and other enzymes involved in the virus life cycle.[4,5] These facts encouraged us to evaluate the activity of *H. bracteatum* leaves methanolic extract, fractions, and the isolated compounds as inhibitors of SARS-CoV-2 M^{pro}.

The methanolic extract exhibited inhibitory activity with IC_{50} value of 14.47 ± 0.74 μg mL^{-1}. Among the tested four fractions, the ethyl acetate fraction showed the highest inhibitory activity followed by petroleum ether, methylene chloride, and butanol fractions with IC_{50} values of 2.589, 3.466, 16.05, and 21.9 μg mL^{-1}, respectively, compared with the standard antiviral compound lopinavir with an IC_{50} value of 0.225 ± 0.01 μM (Table S4 and Fig. S55†).

The isolated compounds (**1–18**) were evaluated for their inhibitory activities against SARS-CoV-2 M^{pro}. Compounds **6**, **12**, and **14** showed comparable inhibitory activities against SARS-COV-2 M^{pro} with IC_{50} values of 0.917 ± 0.05, 0.476 ± 0.02, and 0.610 ± 0.03 μM, respectively, compared with the control lopinavir with an IC_{50} value of 0.225 ± 0.01 μM. Compounds **2**, **5**, **11**, **13**, & **18** showed moderate inhibitory activities with IC_{50} values in the range of 4–8 μM, while compounds **1**, **7**, **9**, **10**, **15**, & **17** exhibited significant activities with IC_{50} values in the range of 10–16 μM. Compounds **3**, **8**, & **16** showed weak activities with IC_{50} values in the range of 20–28 μM. The lowest activity was reported for compound **4** (IC_{50} value of 89.99 ± 4.59 μM).

Compounds **12**, **14**, and **6** showed the highest inhibitory activity. Compounds **6** and **14** are lignans, while compound **12** is a phenyl propanoid derivative nitrogenated at C2. The three compounds share the presence of the phenyl propanoid part oxygenated at C1 & C3 of the propane moiety and C3′ & C4′ of the phenyl moiety. It seems that the oxygenated phenyl propanoid part is crucial for the inhibitory activity, as revealed by the other tested compounds with moderate and significant activities as phenyl propanoid derivative nitrogenated at C2 (**5**), the flavanone compounds **9** & **13**, and the lignan compound **15**.

Although ethyl acetate & petroleum ether fractions showed better inhibitory activities than that of the methylene chloride fraction, compounds **12**, **14**, & **6** that exhibited the highest inhibitory activities were isolated from the methylene chloride fraction. This may be explained by the antagonistic effect of these compounds together and/or with other constituents.

This study is the first that reports the *in vitro* promising SARS-CoV-2 M^{pro} inhibitory activities of compounds **12**, **14**, & **6** besides the moderate activities of compounds **11**, **13**, & **5** against the M^{pro} enzyme. Compounds **2** & **18** were reported for their promising inhibitory activity against the M^{pro} enzyme through the *in silico* study.[54,55] This study is the first study that proves this promising activity through the *in vitro* assay.

2.3 Molecular docking results

Molecular docking is considered as a tool that can be used for predicting the binding mode of the tested compounds with the targeted enzymes. SARS-CoV-2 main protease (M^{pro}) is an enzyme responsible for proteolysis and releasing the essential functioning peptides. It is a promising target against SARS-CoV-2 due to its importance in the viral life cycle replication. Thus, M^{pro} inhibition can better stop the viral replication and recover the symptoms of COVID-19 disease.[3–5] The crystallographic structure of M^{pro} complexed with the co-crystallized ligand (N3) was downloaded from Protein Data Bank (https://www.rcsb.org, code 6LU7). The molecular docking simulation of the isolated tested compounds (**1–18**) was carried out compared with the co-crystallized inhibitor (N3 ligand) and also with lopinavir (standard) to demonstrate their binding modes and affinities for M^{pro} ($3CL^{pro}$), thus explaining their possible inhibitory activities against M^{pro}. The binding scores and interacting amino acid residues involved in the binding between the tested compounds (**1–18**) and the M^{pro} active pockets beside their IC_{50} values are summarized in Tables 1, S5 and S6.†

Previous studies reported that the amino acid residues involved in the binding of the co-crystallized ligand (N3) with M^{pro} are Thr 26, Gly 143, Glu 166, and Gln 189 through hydrogen bonding.[4,5] Lopinavir, the standard antiviral compound used in this study, showed H-bonding binding with Glu166 & Gln189 amino acid residues of M^{pro} (Fig. S6†). Compounds sharing nearly the same binding mode of the co-crystallized inhibitor (N3) and/or lopinavir with M^{pro} will be considered as potential M^{pro} ($3CL^{pro}$) inhibitors, which can be used to explain the *in vitro* results.

The docking results (Tables 1, S5, S6† and Fig. 2a) showed that the interaction of lopinavir (reference drug, IC_{50} 0.225 ± 0.01 μM) shared the N3 ligand in H-bonding binding with Glu166 & Gln189 amino acid residues. The most potent tested compound **12** (IC_{50} 0.476 ± 0.02 μM & binding energy slightly higher than that of lopinavir −10.79 & −9.61 kcal mol^{-1}, respectively) exhibited four H-bonds with Glu 166, Gln 189, Thr 190, & Arg 188 amino acid residues through the free hydroxyl groups in the phenyl moiety and in the propane diol side chain (Fig. 2b). It shared both lopinavir and N3 ligand in H-bonding binding with Glu 166 & Gln 189 amino acid residues. Compound **14** (IC_{50} 0.61 ± 0.03 μM & binding energy −12.96 kcal mol^{-1} higher than that of lopinavir) exhibited seven H-bonds with Gln 189, Glu 166, Thr 26, Thr 24, Ser 46, & Gly 143 amino acid residues through the free hydroxyl groups of the glucose moiety and the oxygenated phenyl moiety besides the furan moiety (Fig. 2c). It shared both lopinavir and the N3 ligand in H-bonding binding with Gln 189 & Glu 166 amino acid residues; it shared the N3 ligand in binding with Gly 143 and Thr 26 amino acid residues. Compound **6** (IC_{50} 0.917 ± 0.05 μM & binding energy of −9.39 kcal mol^{-1} nearly similar to that of lopinavir) exhibited two H-bonds with Glu 166 & Ser 144 amino acid residues (Fig. 2d). It shared lopinavir in H-bonding binding with the amino acid residue Glu 166.

The other isolated compounds (Tables S5 and S6†) also showed good binding interactions to M^{pro} active site's crucial amino acid residues, which are very close to that of the N3 ligand and the standard lopinavir drug. All the tested compounds shared both lopinavir and N3 ligand in binding with Glu166 amino acid residue through H-bonding except compounds **3** and **4**. Compounds **4**, **5**, and **18** shared both lopinavir and N3 ligand in binding with Gln189 amino acid residue. The results of the docking scores and different interactions with amino acids of the protein pocket (two-dimensional visualization) are shown in Tables S5 and S6.†

Table 1 The SARS-COV-2 M^{pro} inhibition (IC_{50} μM), docking scores of the isolated compounds (**1–18**), and the standard compound (lopinavir)

Compound (code)	*In vitro* SARS-COV-2 M^{pro} IC_{50} μM	Binding energy (kcal mol^{-1}) (docking score)	Compound (code)	*In vitro* SARS-COV-2 M^{pro} IC_{50} μM	Binding energy (kcal mol^{-1}) (docking score)
Lopinavir[a]	0.225 ± 0.01	−9.61			
1	12.51 ± 0.64	−9.99	10	12.83 ± 0.65	−13.45
2	4.185 ± 0.21	−10.29	**11**	5.069 ± 0.26	−12.48
3	20.67 ± 1.05	−10.39	**12**	0.476 ± 0.02	−10.79
4	89.99 ± 4.59	−11.92	**13**	5.565 ± 0.28	−12.81
5	8.532 ± 0.43	−8.97	**14**	0.61 ± 0.03	−12.96
6	0.917 ± 0.05	−9.39	**15**	11.46 ± 0.58	−11.69
7	16.31 ± 0.83	−12.34	**16**	27.5 ± 1.4	−14.34
8	27.86 ± 1.42	−12.69	**17**	10.12 ± 0.52	−15.61
9	11.83 ± 0.6	−11.49	**18**	4.74 ± 0.24	−16.24

[a] The standard used Lopinavir.

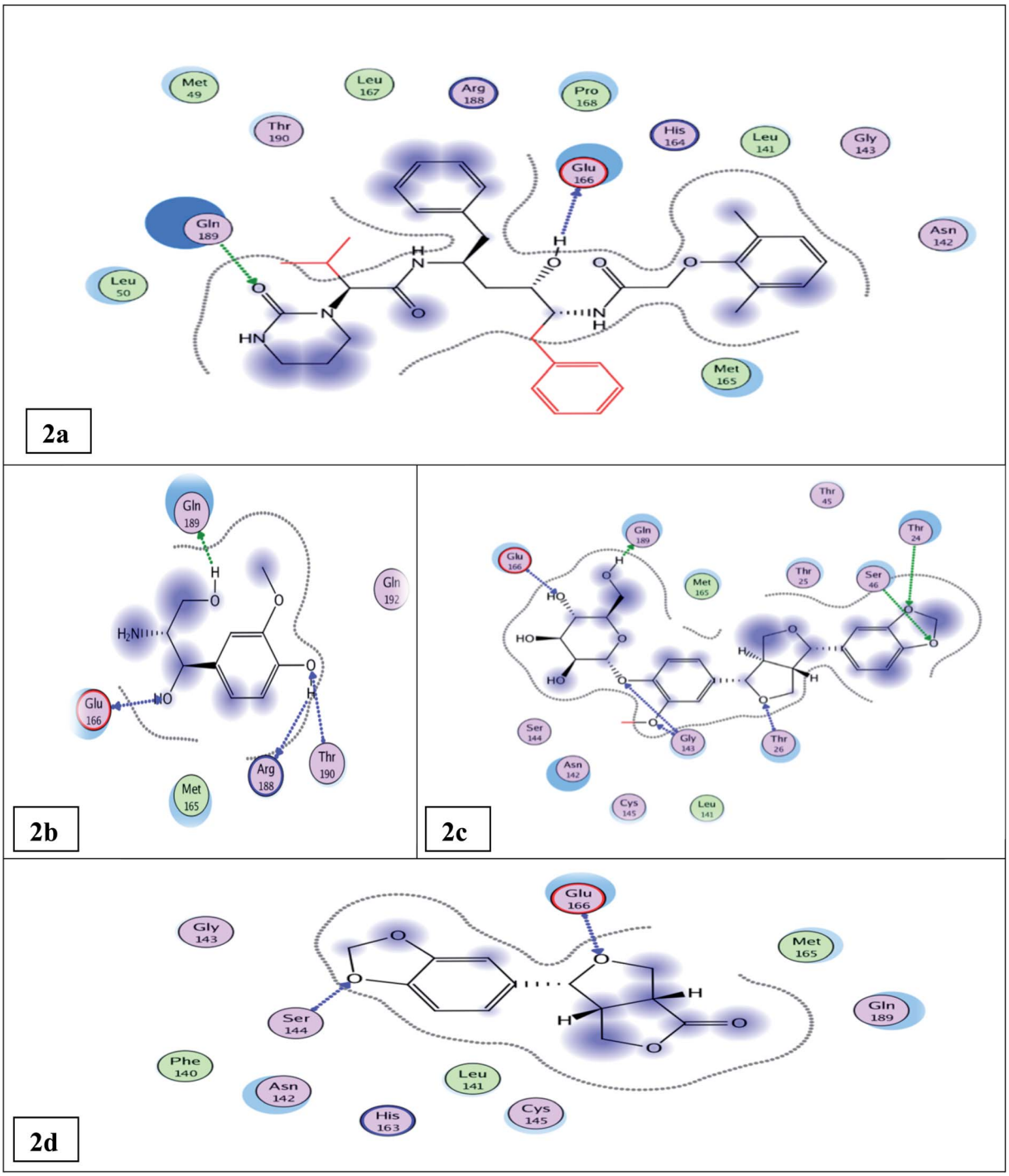

Fig. 2 Docking results of compounds **12**, **14**, **6**, & the standard lopinavir in the active site of SARS-CoV-2 M^{pro} (6LU7). 2D interactions of standard lopinavir (**2a**). 2D interactions of compound **12** (**2b**). 2D interactions of compound **14** (**2c**). 2D interactions of compound **6** (**2d**).

The three-dimensional visualization of the docking results and the binding pocket surface mapping were also shown to simulate ligand binding to the M^{pro} active pocket (Table S7†). Analyzing the docking results of all the tested compounds, compared to the ligand inhibitor N3 of M^{pro} and lopinavir, represented a good idea about their binding modes and affinities. However, the tested compounds showed variable binding strengths, as discussed above.

2.4 Structure activity relationship study

Observing the structure activity relationships of the isolated compounds depending on their binding affinities and binding modes to the M^{pro} pocket and comparing it with their *in vitro* inhibitory activity results against the M^{pro} enzyme compared to lopinavir can give an insight into the characteristic features for the compounds that can be considered as leads for designing

anti-COVID-19 drugs. In this study, generally, compounds **12**, **14**, and **6** achieved nearly the same inhibitory activities against the M^{pro} enzyme compared with lopinavir; they shared the presence of the phenyl propanoid part oxygenated at C1 & C3 of the propane moiety and C3' & C4' of the phenyl moiety, which seemed to be potential sources for developing anti-COVID-19 drugs (Table S5†).

Compounds **5** and **12**, the two phenyl propanoid derivatives nitrogenated at C2 and shared both N3 ligand and lopinavir in binding with both Gln189 and Glu166 amino acid residues, showed different *in vitro* inhibitory activities. This may be attributed to the free hydroxyl group located at C-4′ in compound **12** that increased its binding affinities compared to **5**, where this free phenolic hydroxyl binds by two hydrogen bonds with Thr190 & Arg188 amino acid residues, while the methylenedioxy group in compound **5** binds by only one hydrogen bond with Gln192 (Tables S5 and S6†). This may explain the results of the *in vitro* inhibitory activity assay where compound **12** showed higher inhibitory activity than **5** (IC_{50} value of 0.476 ± 0.02 and 8.532 ± 0.43 μM, respectively) (Fig. S51†).

A careful study of the two lignans **7** and its glucoside **14** revealed that the glucose moiety of compound **14** increased the binding affinities of this compound compared to its aglycone **7** as the glucose moiety in compound **14** shared the N3 ligand and the standard lopinavir in binding by two H-bonds with both Gln189 and Glu166 amino acid residues; in addition, it shared the N3 ligand only in binding by two H-bonds with Gly143 amino acid residue, while the aglycone **7** shared the N3 inhibitor ligand and lopinavir in binding with only Glu 166 amino acid residue (Tables S5 and S6†). This is in agreement with the results of the *in vitro* inhibitory activity assay where compound **14** showed an IC_{50} value of 0.61 ± 0.03 and compound **7** showed an IC_{50} value of 16.31 ± 0.83 (Tables S5 and S6†) (Fig. S53†).

Comparing the binding affinities of the two lignans **14** and **15**, the methylenedioxy group in **14** increased its binding affinities compared with compound **15** that showed two methoxy groups at C-3 & 4 instead of the methylenedioxy group in compound **14**. The methylenedioxy group in compound **14** is bound by the hydrogen bond with two amino acids (Thr 24 & Ser 46), while one of the two methoxy groups in compound **15** is bound by only one hydrogen bond with Thr 26. This matches with the results of the inhibitory activity assay where compound **14** showed an IC_{50} value of 0.61 ± 0.03 μM and compound **15** showed an IC_{50} value of 11.46 ± 0.58 μM (Tables S5 and S6†) (Fig. S54†).

In the steroidal compound **4**, the glucose moiety decreased the activity of this compound compared to its aglycone **1**, where compound **4** showed an IC_{50} value of 89.99 ± 4.59 μM, while **1** showed an IC_{50} value of 12.51 ± 0.64 μM. This revealed that the blocking of the hydroxyl group at the C-3 of sterol decreased the inhibitory activity against M^{pro} ($3CL^{pro}$) (Tables S5 and S6†) (Fig. S52†).

3. Experimental

3.1 Reagents and apparatus

A UV-visible spectrophotometer (Shimadzu 1601 PC, model TCC-240A, Japan) was employed. ESI-HPLC-Mass, TSQ Quantum Access MAX triple stage quadrupole mass spectrometer equipped with an electrospray ionization (ESI) was operated in the positive ionization mode, Thermo Scientific, New York, USA and Accela U-HPLC system using Accela 1250 quaternary pump and Accela open autosampler (operated at 25 °C) New York, USA. Nuclear Magnetic Resonance spectra (^{1}H-NMR, APT, DEPT-Q, HMBC, and HSQC) using TMS as an internal standard were recorded on a Bruker AV-400 spectrometer at 400 MHz for ^{1}H and 100 MHz for ^{13}C NMR. Compounds were dissolved in $CDCl_3$, CD_3OD, or DMSO-d_6. Chemical shifts were given in ppm with a TMS as an internal standard. Column chromatography was performed on silica gel 60 (Merck, Germany) and thin-layer chromatography on precoated silica gel 60 GF_{254} (20 × 20 cm × 0.2 mm thick) on an aluminum sheet (Merck, Germany), RP-C_{18} (Merk, Germany), and Sephadex LH 20 (Pharmacia, USA). Spots were visualized by exposure to vanillin sulfuric spraying reagent.

For the FRET-based activity assay, 3CL Protease (SARS-CoV-2) Assay Kit (Catalog #79955-1) was used to measure the main protease activity. The kit comes in a convenient 96-well format with purified main protease, fluorogenic substrate, and main protease assay buffer for 100 enzyme reactions. Also, lopinavir was included as a positive control. In addition, microtiter plate-reading fluorimeter was used to measure the fluorescence intensity.

(6042 Cornerstone Court West, Ste. BSan Diego CA 92121, Email: info@bpsbioscience.com).

3.2 Preparation of the plant material

The aerial parts of *H. bracteatum* ornamental plant were collected from El-Orman Garden, Cairo, Egypt in June 2019. The plant identity was confirmed by Associate Prof. Dr Mahmoud Makram Qassem, Department of Vegetables & Floriculture, Faculty of Agriculture, Mansoura University, Egypt. Voucher specimens were coded as Hb-1-2019 and kept in Pharmacognosy Department, Faculty of Pharmacy, Mansoura University, Egypt.

3.3 Extraction and isolation

The leaves of the plant were separated, air dried in shade, and then powdered. The dried powdered leaves (2.5 kg) were extracted with 70% hydro-alcoholic methanol (6 × 10 L) by maceration. The collected methanolic extracts were evaporated under reduced pressure to give (444 g) of a dark green viscous residue. The dried methanolic extract was dissolved in the least amount of methanol, diluted with 1000 mL distilled water, fractionated using solvents of increasing polarities such as petroleum ether (12 × 500 mL), methylene chloride (10 × 500 mL), ethyl acetate (9 × 500 mL), and finally with *n*-butanol (5 × 300 mL). The solvent, in each case, was evaporated to dryness under reduced pressure giving petroleum ether extract (115 g), methylene chloride extract (150 g), ethyl acetate extract (19 g), and *n*-butanol extract (17 g). The petroleum ether extract (70 g) was subjected to normal silica gel column chromatography, eluted with petroleum ether : ethyl acetate (100 : 0) till (0 : 100), and then ethyl acetate : methanol (100 : 0) till (0 : 100) to give

two groups, namely, group 1 and group 2. Group 1, eluted with petroleum ether : ethyl acetate (90 : 10), when left for crystallization, precipitated a white powder (compound **1**, 14 mg), while the supernatant was collected, dried, and then re-chromatographed over normal silica gel column using petroleum ether : ethyl acetate (100 : 0) till (0 : 100) to give two subgroups 1A and 1B; subgroup 1A (fractions 28–43), eluted with petroleum ether : ethyl acetate (98 : 2), was also re-chromatographed over a normal silica gel column using petroleum ether : ethyl acetate (100 : 0) till (0 : 100) and yielded sub-fractions (41–49), eluted with petroleum ether : ethyl acetate (88 : 12), which produced compound **2**, 5 mg, while subgroup 1B (fractions 81–103) was further re-chromatographed over normal silica gel column using petroleum ether : methylene chloride (100 : 0) till (0 : 100), yielded sub-fractions (103–109), eluted with methylene chloride (100%), produced compound **3**, 5 mg. Group 2, eluted with petroleum ether : ethyl acetate (20 : 80), was re-chromatographed over a normal silica gel column using methylene chloride : methanol (100 : 0 till 0 : 100), sub-fractions (35–49), eluted with methylene chloride : methanol (96 : 4), when left for crystallization, white substance precipitated (compound **4**, 86 mg).

Methylene chloride extract (120 g) was subjected to normal silica gel column chromatography, elution was carried out using petroleum ether : ethyl acetate (100 : 0) till (0 : 100) then ethyl acetate-methanol (100 : 0) till (0 : 100) to give seven groups 1–7. Group 1 (fractions 81–97), eluted with petroleum ether : ethyl acetate (88 : 12), was re-chromatographed over a normal silica gel column using petroleum ether : ethyl acetate (94 : 6) to yield sub-fractions (33–39), when left for crystallization, precipitated a white substance (compound **5**; 13 mg). Group 2 (fractions 139–155), eluted with petroleum ether : ethyl acetate (79 : 21), was re-chromatographed over normal silica gel column using petroleum ether : methylene chloride (60 : 40 till 0 : 100) for elution; two subgroups were obtained, namely, 2A and 2B. Subgroup 2A (fractions 65–80), eluted with petroleum ether : methylene chloride (95 : 5), when left for crystallization, precipitated a white needle substance (compound **6**; 7 mg). Subgroup 2B (fractions 121–125), eluted with methylene chloride (100%), was re-chromatographed over normal silica gel column using petroleum ether : methylene chloride (50 : 50 till 0 : 100) for elution giving fractions (30–52), eluted with petroleum ether : methylene chloride (10 : 90), when left for crystallization, a white substance was precipitated (compound **7**; 1 g). Group 3 (fractions 168–175), eluted with petroleum ether : ethyl acetate (76 : 24), was re-chromatographed over normal a silica gel column using methylene chloride : methanol (99 : 1) using isocratic elution, yielded two subgroups 3A and 3B. Subgroup 3A (fraction 9) was re-chromatographed over normal silica gel preparative TLC using methylene chloride : methanol (98 : 2), when left for crystallization, precipitated a yellowish white substance (compound **8**; 7 mg). Subgroup 3B (fractions 50–80), when left for crystallization, precipitated a yellowish white substance (compound **9**; 33 mg). Group 4 (fractions 180–200), eluted with petroleum ether : ethyl acetate (73 : 27), when left for crystallization, precipitated a yellow substance (compound **10**; 20 mg). Group 5 (fractions 208–230), eluted with petroleum ether : ethyl acetate (70 : 30), was re-chromatographed over normal silica gel column using methylene chloride : methanol (100 : 0 till 98 : 2) to elute fractions (36–39), when left for crystallization, precipitated yellow substance (compound **11**; 6 mg). Group 6 (fractions 243–276), eluted with petroleum ether : ethyl acetate (67 : 33), was re-chromatographed over normal silica gel column using petroleum ether : methylene chloride (5 : 95 till 0 : 100) then methylene chloride : methanol (100 : 0 till 0 : 100) yielded two subgroups 6A and 6B. Subgroup 6A (fractions 60–75), eluted with methylene chloride (100%), when left for crystallization, precipitated colorless needles (compound **12**; 10 mg), while subgroup 6B (fractions 119–131), eluted with methylene chloride : methanol (98 : 2), when left for crystallization, a yellow powder precipitated (compound **13**, 6 mg). Group 7 (fractions 360–375), eluted with ethyl acetate : methanol (95 : 5), was re-chromatographed over a normal silica gel column using methylene chloride : methanol (100 : 0 till 0 : 100) and produced two subgroups 7A and 7B. Subgroup 7A (fractions 31–41), eluted with methylene chloride : methanol (96 : 4), when left for crystallization, a white powder precipitated (compound **14**, 1.5 g). Subgroup 7B (fractions 42–50), also eluted with methylene chloride : methanol (96 : 4), was re-chromatographed over normal silica gel preparative TLC using methylene chloride : methanol (90 : 10), when left for crystallization, a white substance precipitated (compound **15**, 5 mg).

The ethyl acetate extract (15 g) was subjected to normal silica gel column chromatography, eluting with ethyl acetate : methanol (100 : 0) till (0 : 100) to give two groups: group 1 and group 2. Group 1 (fractions 26–39), eluted with ethyl acetate: methanol (95 : 5), when left for crystallization, precipitated a yellow substance (compound **16**, 65 mg). Group 2 (fractions 40–45), also eluted with ethyl acetate : methanol (95 : 5), was re-chromatographed over a Sephadex LH 20 column using methanol (100%), yielded two subgroups 2A and 2B. Subgroup 2A (fractions 28–37), which was re-chromatographed over normal silica gel column using methylene chloride : methanol (100 : 0 till 0 : 100) to give sub-fractions (50–100), eluted with methylene chloride : methanol (85 : 15), when left for crystallization, precipitated a yellow powder (compound **17**, 5 mg). Subgroup 2B (fractions 43–70) was re-chromatographed over reversed silica gel column RP-C_{18} using water : methanol (100 : 0 till 0 : 100), yielded fractions (17–23), eluted with water : methanol (95 : 5), when left for crystallization, a yellow substance was precipitated (compound **18**, 7 mg).

3.4 FRET-based activity assay (Fluorescence Resonance Energy Transfer assay)

The inhibitory activity against the SARS-CoV-2 main protease (M^{pro} or $3CL^{pro}$) assay was carried out based on the FRET-based activity assay.[56] The principle of the assay depends on the C-terminal of the peptide substrate being linked to a fluorophore (Edans) and the N-terminal has a fluorescence quencher (Dabcyl) that quenches the fluorescence signal of Edans. Thus, the peptide substrate exhibits low fluorescence because the fluorescence intensity of Edans in the C-terminal is quenched by the Dabcyl in the N-terminal of the substrate.

When the M^{pro} hydrolyzes the substrate, it yields two fragments: non-fluorescent Dabcyl fragment and highly florescent Edans fragment. Consequently, an increase in the fluorescence signal proportional to the protease activity occurs. Main protease (M^{pro}) inhibitor causes the inhibition of fluorescent fragment release, and thus decrease intensity of the fluorescence signal. Fluorescence intensity is measured with a fluorescent microtiter plate reader capable of reading excitation/emission = 360/460 nm.[57]

3.5 Molecular modelling simulation study

The binding affinities of the isolated compounds **1–18** to SARS-CoV-2 main protease (M^{pro}) pocket amino acids residues were predicted by carrying out a docking experiment for them and comparing their results with the co-crystallized ligand (N3 inhibitor)[4] and the standard lopinavir. Lopinavir was previously reported for its promising inhibitory activity against SARS-COV-2 M^{pro} enzyme through *in silico* computational study[58] and it was also reported for inhibiting SARS-CoV-2 replication *in vitro* study.[59]

3.5.1 Ligand and protein preparation. The structures of compounds (**1–18**) that was docked in their neutral forms were built using the builder of Molecular Operating Environment (MOE) version 2009.10 (Chemical Computing Group Inc. software. **https://www.chemcomp.com**). Ligands (the structures that will be docked) were prepared for docking by minimizing their energy to get the most stable conformers of ligands and they were imported and saved in the form of MDB file to be ready for docking into the M^{pro} active site. For protein preparation, the crystal structure was protonated, hydrogen atoms were added, an automatic correction to check for any errors in the atom's connection and the type was applied, and the fixation of the potential of the receptor and its atoms was done. Site Finder was used for the selection of the same active site of the co-crystallized inhibitor in the protease structure using all default items and dummy atoms of the pocket were created. The program specifications were adjusted so that the docking site was specified as dummy atoms, triangle matcher as the placement methodology, and London dG as the scoring methodology for the selection of the best 19 poses from 380 different poses for each tested compound. The isolated compounds were docked into the binding site of the M^{pro} enzyme; PDB code ID 6LU7 was used as the target enzyme.

3.5.2 Molecular modeling visualization. All the visualization of the docking files was done using MOE software. After the completion of the docking processes, the obtained poses were studied. The best compounds are those showing the more negative docking scores that refer to the better capability of a compound to dock with the target and make more desirable ligand–enzyme interactions.[4]

4. Conclusion

The methanolic extract, petroleum ether, methylene chloride, and ethyl acetate fractions of *H. bracteatum* leaves besides eighteen isolated and identified compounds (**1–18**) were *in vitro* evaluated for their inhibitory activities against SARS-CoV-2 main protease (M^{pro}) using fluorescence resonance energy transfer assay (FRET-based assay). The tested isolated compounds (**1–18**) included phenylpropanoid derivatives nitrogenated at C-2, lignans, and rare flavonoids. The methanolic extract and fractions exhibited promising inhibitory activities. Compounds **6**, **12**, and **14** showed comparable inhibitory activities against SARS-COV-2 M^{pro} with IC_{50} values of 0.917 ± 0.05, 0.476 ± 0.02, and 0.610 ± 0.03 μM, respectively, compared with the control lopinavir with an IC_{50} value of 0.225 ± 0.01 μM. The other tested compounds showed significant inhibitory activities. Thus, the methanolic extract of *H. bracteatum* leaves and the isolated phenylpropanoid derivatives, lignans, followed by flavonoids, could be considered promising natural SARS-COV-2 M^{pro} inhibitors. The molecular docking study for the tested compounds was carried out to correlate their binding modes and affinities for M^{pro} enzyme with the *in vitro* results. Combining the results of the *in vitro* and *in silico* studies led us to suggest the structural basis of potential inhibitors targeting SARS-COV-2 M^{pro}. It could be concluded that phenylpropanoids skeleton oxygenated at C3, C4 of the phenyl moiety and at C1, C3 of the propane part is the essential core of the SARS-COV-2 M^{pro} inhibitors and could be considered during the isolation of natural compounds, semi-synthesis, or synthesis of effective anti-COVID-19 drugs.

Conflicts of interest

We declare that we have no conflict of interest.

Acknowledgements

The authors would like to acknowledge assistant lecturers Mohamed A. Sabry and Eman T. Warda, for helping in molecular docking study.

References

1 F. Wu, S. Zhao, B. Yu, Y. Chen, W. Wang, Z. Song, Y. Hu, Z. Tao, J. Tian, Y. Pei, M. Yuan, Y. Zhang, F. Dai, Y. Liu, Q. Wang, J. Zheng, L. Xu, E. C. Holmes and Y. Zhang, *Nature*, 2020, **579**, 265–284.
2 B. Hu, H. Guo, P. Zhou and Z. Sh, *Nat. Rev. Microbiol.*, 2021, **19**, 141–154.
3 J. Huang, G. Tao, J. Liu, J. Cai, Z. Huang and J. Chen, *Front. Pharmacol.*, 2020, **11**, 588508.
4 A. A. Zaki, A. A. Al-Karmalawy, Y. A. El-Amier and A. Ashour, *New J. Chem.*, 2020, **44**, 16752–16758.
5 A. E. Allam, Y. Amen, A. Ashour, H. K. Assaf, H. A. Hassan, I. M. Abdel-Rahman, A. M. Sayed and K. Shimizu, *RSC Adv.*, 2021, **11**, 22398.
6 J. O. Ogidigo, E. A. Iwuchukwu, C. U. Ibeji, O. Okpalefe and M. E. S. Soliman, *J. Biomol. Struct. Dyn.*, 2022, **40**(5), 2284–2301.
7 A. Zrig, *Pharm. Chem. J.*, 2022, **55**(10), 1080–1084.

8 A. M. Kakam, K. Franke, J. C. Ndom, E. Dongo, T. N. Mpondo and L. A. Wessjohann, *Biochem. Syst. Ecol.*, 2011, **39**, 166–167.
9 D. A. Viegas, A. Palmeira-de-Oliveira, L. Salgueiro, J. Martinez-de-Oliveira and R. Palmeira-de-Oliveira, *J. Ethnopharmacol.*, 2014, **151**, 54–65.
10 I. Kutluk, M. Aslanb, I. E. Orhan and B. Özçelik, *S. Afr. J. Bot.*, 2018, **119**, 252–257.
11 M. Leonardi, S. Giovanelli, K. E. Ambryszewska, B. Ruffoni, C. Cervelli, L. Pistelli, G. Flamini and L. Pistelli, *Biochem. Syst. Ecol.*, 2018, **79**, 15–20.
12 B. Najar, C. Cervelli, B. Ferri, P. L. Cioni and L. Pistelli, *S. Afr. J. Bot.*, 2019, **124**, 178–187.
13 J. Werner, W. Ebrahim, F. C. Özkaya, A. Mándi, T. Kurtán, M. El-Neketi, Z. Liu and P. Proksch, *Fitoterapia*, 2019, **133**, 80–84.
14 G. Appendino, M. Ottino, N. Marquez, F. Bianchi, A. Giana, M. Ballero, O. Sterner, B. L. Fiebich and E. Munoz, *J. Nat. Prod.*, 2007, **70**, 608–612.
15 S. Verma, D. Twilley, T. Esmear, C. B. Oosthuizen, A. Reid, M. Nel and N. Lall, *Front. Pharmacol.*, 2020, **11**, 561334.
16 L. Bailey and the staff of the Bailey hortorium, *Manual of cultivated plants*, Macmillan Publishing Co. Inc., New York, 5th edn, 1975, pp. 318–320.
17 W. Kisiel, *Planta Med.*, 1980, **38**(3), 285–287.
18 R. Gunasegaran, A. Ubeda, M. J. Alcaraz, R. Jayaprakasam and A. G. Nair Ramachandran, *Pharmazie*, 1993, **48**(3), 230–231.
19 H. Liu, H. He, X. Yang, M. Chen and X. Hao, *Nat. Prod. Res. Dev.*, 2007, **19**(3), 423–426.
20 S. G. Leitao, M. A. C. Kaplan, F. D. Monache, T. Akii-Iisa and T. Tamura, *Phytochemistry*, 1992, **31**(8), 2813–2817.
21 V. D. Ebajo Jr, C. Shen and C. Y. Ragasa, *J. Appl. Pharm. Sci.*, 2015, **5**(4), 33–39.
22 S. B. Mahato and A. P. Kundu, *Phytochemistry*, 1994, **37**, 1517–1575.
23 M. E. D. Pietro, A. Mannu and A. Mele, *Processes*, 2020, **8**, 410.
24 R. G. Powell, C. R. Smith and I. A. Wolff, *J. Am. Oil Chem. Soc.*, 1965, **42**(3), 165–169.
25 A. R. Kim, H. J. Ko, M. A. Chowdhury, Y. Chang and E. Woo, *Arch. Pharmacal Res.*, 2015, **38**(6), 1059–1065.
26 S. E. Cellitti, D. H. Jones, L. Lagpacan, X. Hao, Q. Zhang, H. Hu, S. M. Brittain, A. Brinker, J. Caldwell, B. Bursulaya, G. Spraggon, A. Brock, Y. Ryu, T. Uno, P. G. Schultz and B. H. Geierstanger, *J. Am. Chem. Soc.*, 2008, **130**, 9268–9281.
27 F. Labeda, M. Masullob, A. Cerullib, F. Benayachea, S. Benayachea and S. Piacenteb, *Nat. Prod. Commun.*, 2017, **12**, 1605–1608.
28 W. D. Macrare and G. H. N. Towers, *Phytochemistry*, 1985, **24**, 561–566.
29 M. Chiba, S. Hisada, S. Nishibe and H. Thieme, *Phytochemistry*, 1980, **19**, 335–336.
30 H. J. Lee, S. M. Seo, O. K. Lee, H. J. Jo, H. Y. Kang, D. H. Choi, K. H. Paik and M. Khan, *Helv. Chim. Acta*, 2008, **9**, 2361–2366.
31 T. Lida, Y. Noro and K. Ito, *Phytochemistry*, 1983, **22**(1), 211–213.
32 N. Takaku, D. Choi, K. Mikame, T. Okunishi, S. Suzuki, H. Ohashi, T. Umezawa and M. Shimada, *J. Wood Sci.*, 2001, **47**, 476–482.
33 S. W. Yoo, J. S. Kim, S. S. Kang, K. H. Son, H. W. Chang, H. P. Kim, K. Bae and C. Lee, *Arch. Pharmacal Res.*, 2002, **25**(6), 824–830.
34 M. Kim, H. T. Moon, D. G. Lee and E. Woo, *Arch. Pharmacal Res.*, 2007, **30**(4), 425–430.
35 V. Atabakia, J. Pourahmad and T. Hosseinabadia, *S. Afr. J. Bot.*, 2021, **137**, 399–405.
36 R. Saladino, C. Fiani, C. Crestini, D. S. Argyropoulos, S. Marini and M. Coletta, *J. Nat. Prod.*, 2007, **70**, 39–42.
37 J. Jakupovic, V. P. Pathak, F. Bohlmann, R. M. King and H. Robinson, *Phytochemistry*, 1987, **26**(3), 803–807.
38 T. Mabry, K. Markham and M. Thomas, *The systematic identification of flavonoids*, Springer-Verlag, Berlin, Heidelberg and New York, 1970.
39 K. R. Markham, *Techniques of Flavonoid Identification, Biological Technique Series*, Academic Press Inc., London and New York, 1982.
40 J. B. Harborne and T. J. Mabry, *The Flavonoids: Advances in Research*, Champan and Hall Ltd, 1982.
41 P. Agrawal, R. Thakur and M. Bansal, *Carbon-^{13}NMR of flavonoids*, Elsevier Science Publishing Company Inc., 1989.
42 S. Takagi, M. Yamaki and K. Inoue, *Yakugaku Zasshi*, 1980, **100**(12), 1220–1224.
43 A.-u. -Rahman, S. Hareem, M. I. Choudhary, B. Sener, A. Abbaskhan, H. Siddiqui, S. Anjum, I. Orhan, I. Gurbuz and F. Ayanoglud, *Heterocycles*, 2010, **82**(1), 813–824.
44 J. N. Lee, C. M. Lee, G. T. Lee and G. G. Lee, *Repub. Korean Kongkae Taeho Kongbo*, KR 2012078097 A 20120710, 2012.
45 J. N. Lee, C. M. Lee, G. T. Lee and G. G. Lee, *Repub. Korean Kongkae Taeho Kongbo*, KR2012078095 A 20120710, 2012.
46 A. Suzuki, O. Shirota, K. Mori, S. Sekita, H. Fuchino, A. Takano and M. Kuroyanagi, *Chem. Pharm. Bull.*, 2009, **57**(3), 245–251.
47 D. K. Bhardwaj, A. K. Gupta, R. K. Jain and G. C. Sharma, *Curr. Sci.*, 1978, **47**(12), 424–425.
48 M. Krishnamurti, T. R. Seshadri and N. D. Sharma, *Indian J. Chem.*, 1971, **9**(2), 189–190.
49 J. Jang, H. P. Kim and H. Park, *Arch. Pharmacal Res.*, 2005, **28**(8), 877–884.
50 J. Yang, Y. S. Kwon and M. J. Kim, *Arabian J. Chem.*, 2015, **8**, 407–413.
51 T. Morikawa, L. Wang, S. Nakamura, K. Ninomiya, E. Yokoyama, H. Matsuda, O. Muraoka, L. Wu and M. Yoshikawa, *Chem. Pharm. Bull.*, 2009, **57**(4), 361–367.
52 L. Verotta, L. Belvisi, V. Bertacche and M. C. Loi, *Nat. Prod. Commun.*, 2008, **3**(12), 2037–2042.
53 B. D'Abrosca, E. Buommino, G. D'Angelo, L. Coretti, M. Scognamiglio, V. Severino, S. Pacifico, G. Donnarumma and A. Fiorentino, *Bioorg. Med. Chem.*, 2013, **21**, 7038–7046.
54 M. C. Ali, A. J. Nur, S. S. Khatun, R. Dash, M. M. Rahman and M. M. Karim, *J. Adv. Biotechnol. Exp Ther.*, 2020, **3**(4), 57–67.

55 S. Shah, D. Chaple, S. Arora, S. Yende, C. Mehta and U. Nayak, *J. Biomol. Struct. Dyn.*, 2021, 1–10.
56 J. S. Morse, T. Lalonde, S. Xu and W. R. Liu, *Chembiochem*, 2020, **21**(5), 730–738.
57 W. Zhu, X. M. Miao, C. Z. Chen, H. Guo, M. Shen, X. Hu, P. Shinn, C. Klumpp-Thomas, S. G. Michael and W. Zheng, *ACS Pharmacol. Transl. Sci.*, 2020, **3**(5), 1008–1016.
58 K. A. Peele, C. P. Durthi, T. Srihansa, S. Krupanidhi, A. V. Sai, D. J. Babu, M. Indira, A. R. Reddy and T. C. Venkateswarulu, *Inform. Med. Unlocked*, 2020, **19**, 100345.
59 K. Choy, A. Y. Wong, P. Kaewpreedee, S. F. Sia, D. Chen, K. P. Y. Hui, D. K. W. Chu, M. C. W. Chan, P. P. Cheung, X. Huang, M. Peiris and H. Yen, *Antiviral Res.*, 2020, **178**, 104786.